Biointerface Research in Applied Chemistry
Open-Access Journal (ISSN: 2069-5837)

Article
Volume 16, Issue 1, 2026, 31
https://doi.org/10.33263/BRIAC161.031

Computational Exploration of Bcl-2 Inhibitors from *Codiaeum variegatum*: Docking, MD, and DFT Analyses

Wirdatun Nafisah [1,*], Gusnia Meilin Gholam [2,3], Maheswari Alfira Dwicesaria [2], Elma Sakinatus Sajidah [1], Fatima Shahid [4,5], Yelin Adalina [3], Dimas Andrianto [2], I Made Artika [2]

1 Biology Department, Faculty of Mathematics and Natural Science, Universitas Negeri Surabaya, Indonesia
2 Department of Biochemistry, Faculty of Mathematics and Natural Sciences, Bogor Agricultural University, Dramaga Campus, Bogor 16680, Indonesia
3 Research Center for Applied Botany, National Research and Innovation Agency (BRIN), Jl. Raya Jakarta-Bogor Km. 46, Cibinong, Bogor, Jawa Barat - 16911, Indonesia
4 Department of Applied Physics, Faculty of Science and Technology, FST, University Kebangsaan Malaysia (UKM), Malaysia
5 Department of Industrial Biotechnology, Atta Ur Rahman School of Applied Biosciences, National University of Sciences and Technology, Islamabad, Pakistan
* Correspondence: wirdatunnafisah@unesa.ac.id;

Received: 20.06.2025; Accepted: 18.12.2025; Published: 15.02.2026

Abstract: Cancer remains a major health issue, and Bcl-2 inhibits apoptosis. This study explored *the phytochemicals of Codiaeum variegatum* as potential Bcl-2 inhibitors. Receptor–ligand docking was conducted with YASARA, followed by 300 ns MD using AMBER14. ADME and DFT analyses were used to characterize the pharmacokinetics and electronic properties of the inhibitor candidates. The large-scale data generated from the 300-nanosecond MD simulations were further processed to map the energy landscapes using PCA and DCCM analysis in R Studio. We successfully applied the QM-AM1 method to the preparation and execution of molecular docking studies. Among the 17 phytochemical compounds isolated from *C. variegatum*, taraxerol demonstrated the most promising binding energy, with a docking score of −8.868 kcal/mol, which is comparable to that of the co-crystallized reference ligand, venetoclax. Taraxerol also satisfied the ADME criteria based on Lipinski's Rule of Five, with only a single rule violation, and DFT calculations confirmed its stability, exhibiting an energy gap of −0.1805 eV. Furthermore, a 300 ns MD simulation revealed that the binding energy of taraxerol, computed using the MM-PBSA method, was more favorable than that of venetoclax, with taraxerol yielding 303.235 kJ/mol in complex with Bcl-2, compared to 291.115 kJ/mol for venetoclax. PCA and DCCM analyses additionally supported the dynamic stability of taraxerol as a potential Bcl-2 inhibitor. Although ADME predictions suggest a favorable safety profile, further *in vitro* and *in vivo* validation is required to substantiate its therapeutic potential.

Keywords: Bcl 2; HOMO-LUMO; principal component analysis; DCCM; *Codiaeum variegatum*.

1. Introduction

Cancer represents a serious global health challenge, with an estimated 52,900 new cases and 27,000 deaths each day. By 2040, it is projected that the number of new cancer cases will rise to 28 million annually, with 16.2 million cancer-related deaths worldwide [1]. Therefore, cancer is categorized as a chronic disease due to its highly complex nature, involving various

alterations in multiple genes at the molecular level [2]. Cancer is caused by a variety of factors that lead to abnormal cell growth or genetic mutations [3]. Currently, there is growing concern due to the increasing body of evidence indicating that nearly all malignancies (cancers) can be associated with resistance to apoptosis. Divergent mechanisms of tumor progression have been reported across cancer types; however, a central hallmark involves dysregulation of apoptosis mediated by the Bcl-2 (B-cell lymphoma-2) protein family. Numerous studies have documented that many tumors exhibit elevated expression of anti-apoptotic Bcl-2 members, both at initial diagnosis and during the development of therapeutic resistance, whereas pro-apoptotic members are often concomitantly downregulated. This imbalance impairs mitochondria-mediated apoptosis, making Bcl-2 an attractive and extensively investigated target for anticancer therapy. Venetoclax, a clinically approved Bcl-2 inhibitor, exemplifies this strategy by reactivating BAX/BAK-dependent mitochondrial pore formation, promoting cytochrome c release, and ultimately restoring programmed cell death [4].

Codiaeum variegatum (*C. variegatum*) is a widely distributed medicinal plant belonging to the Euphorbiaceae family. Its leaves, roots, and stems contain diverse phytochemicals, whose composition varies by plant variety and geographical origin. Previous studies have documented several pharmacological activities, including anti-diarrheal, anti-inflammatory, antiviral, antimicrobial, antioxidant, and antifungal effects [5]. Natural compounds have remained a leading research focus in the search for Bcl-2 inhibitors. Recently, phytochemicals from *W. trilobata* were reported as potential Bcl-2 inhibitors using an *in silico* computational approach. Using similar computational strategies, two additional compounds have also been identified in previous studies for their potential to interact with and inhibit Bcl-2. The exploration of natural compounds as Bcl-2 inhibitors continues to gain momentum and represents a rapidly expanding area of research [6–8].

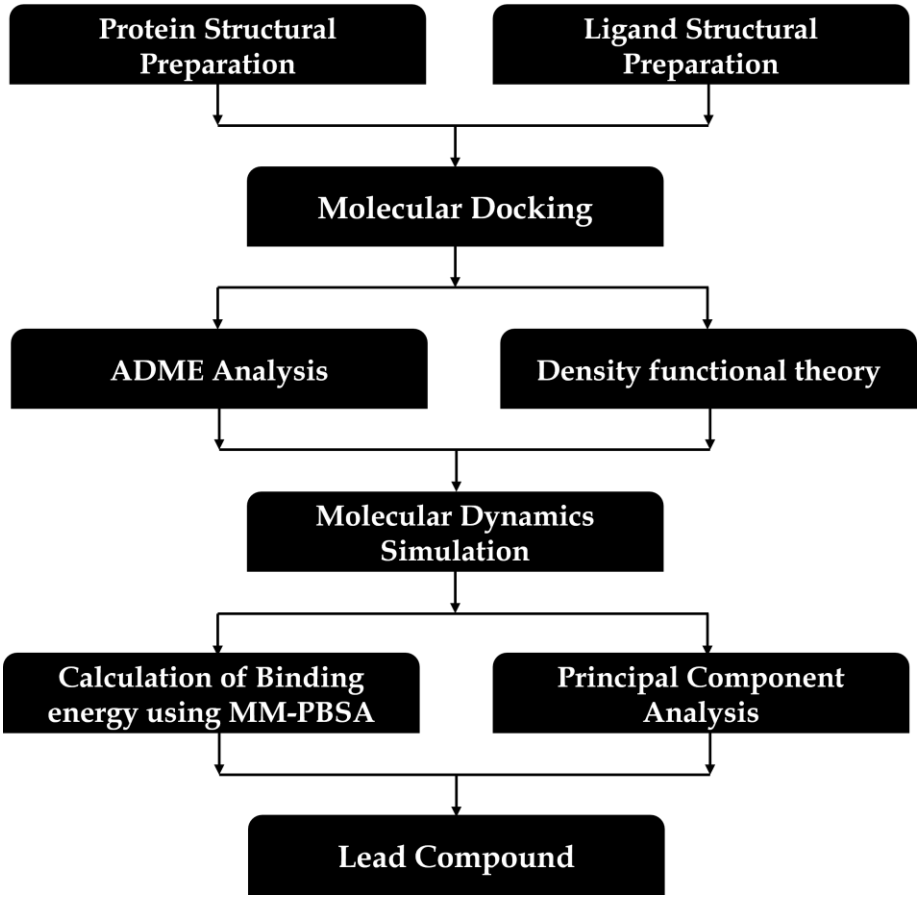

Figure 1. Schematic diagram depicting the workflow adopted to carry out this study.

Although *C. variegatum* has long been used in Traditional Chinese Medicine (TCM), particularly in southern China, no investigations have evaluated its potential as a Bcl-2 inhibitor. Therefore, this study employed an *in silico* computational approach to identify the phytochemical constituents of *C. variegatum* that may serve as novel Bcl-2 inhibitor candidates in the search for new anticancer agents. The workflow of this study is illustrated in Figure 1. In this study, *in silico* approaches were employed to systematically identify, characterize, and prioritize potential Bcl-2 inhibitors before entering costly and time-consuming laboratory testing. Computational techniques such as molecular docking, molecular dynamics simulations, ADME prediction, and MM-PBSA were selected because they enable a rapid, mechanistic evaluation of ligand–receptor interactions, binding energetics, and pharmacokinetic liabilities. These tools allow us to predict how candidate molecules engage the Bcl-2 binding pocket, assess the stability and feasibility of the resulting complexes, and estimate whether a compound possesses drug-like properties suitable for further development [9–13].

2. Materials and Methods

2.1. Protein structural preparation.

This study utilized the Bcl-2 receptor with the PDB ID 6O0K (rcsb.org/structure/6O0K) [14]. The receptor was prepared using the YASARA structure (Version 19.9.17) by removing water molecules and adding hydrogen atoms. The receptor was conditioned under default pH settings, and the AMBER14 force field was applied. The prepared Bcl-2 structure was then stored in (.pdb) format for subsequent analyses [15,16].

2.2. Ligand structural preparation.

The structures of the investigated compounds and the control drug were obtained by downloading them from PubChem (pubchem.ncbi.nlm.nih.gov/) in (.sdf) format. These compounds were then prepared using the YASARA structure (Version 19.9.17) by adding hydrogen atoms, setting the pH to default, and applying the QM-AM1 method. The list of investigated compounds from *C. variegatum* was sourced from a literature study by Pandey and Singh [5]. For the optimization method, we chose semi-empirical quantum mechanics and finalized the structures through energy minimization. Each structure was saved in (.pdb) format. Finally, the structures were converted into (*_ligands.sdf) format, which includes the investigated compounds and control drug [15,16].

2.3. Molecular docking.

Molecular docking was performed using the YASARA structure (Version 19.9.17), implementing the VINA method by running the command via the dock_runscreening macro. In this macro, we set the number of runs to 25 and applied the AMBER14 force field. The Bcl-2 receptor, uploaded into the YASARA structure (Version 19.9.17), was further prepared using the AMBER14 force field, and Bcl-2 was positioned in a rigid state. The structure was then saved in *the* (_receptor.sce) format. The compounds stored in (_ligands.sdf) format were then run to target Bcl-2 with grid box sizes of X-52.59, Y-52.59, and Z-52.59 Å. Subsequently, the docking results were saved in the (*_complex.sce) format. After completing these procedures, the docking run was initiated using the prepared macro. Data retrieval from the docking results,

along with 2D and 3D visualizations, was facilitated using BIOVIA Discovery Studio (Dassault Systèmes, Version: 24.1) in this study [17,18].

2.4. ADME study.

From the docking results, we selected the control drug and top test ligand for further analysis of their ADME properties using the SwissADME (swissadme.ch/) approach. To obtain the ADME data, we uploaded the SMILES strings, which were obtained from PubChem (pubchem.ncbi.nlm.nih.gov/) [19].

2.5. Density functional theory (DFT).

The DFT running process in this study was performed using ORCA (Version 5.0.0) to obtain the highest occupied molecular orbital (HOMO) energy (E_{HOMO}) and lowest unoccupied molecular orbital (LUMO) energy (E_{LUMO}) for the control drug and top test ligand. These compounds were prepared using Avogadro (version 1.2.0) to achieve the optimal energy for each ligand. The input parameters for running ORCA were set to perform geometry optimization using the DFT method with the def2-SVP basis set. The selection of this basis set was made because it has been previously employed in studies aimed at identifying anticancer compounds [20]. The resulting structures were saved in (.inp) format for the DFT computation process. Once the DFT computation was completed, we used IboView (v20211019) to obtain the E_{HOMO} and E_{LUMO} values.

2.6. Molecular dynamics.

We then conducted molecular dynamics (MD) simulations using the YASARA Structure (Version 19.9.17) software with a 300 ns trajectory. 300 ns was selected to enable the exploration of a longer simulation trajectory and to allow for a more comprehensive evaluation. Current studies typically rely only on 100-ns trajectories [21–23]. MD simulations were performed on the top ligand and the control drug. An assisted model building with an energy refinement (AMBER14) force field was applied for the MD simulation. Several settings were implemented, including 0.9% NaCl, a temperature of 310 K, and an extension of the cell by 10 Å. To run the MD simulation, we used the *md_run* macro, while the evaluation of the large simulation dataset was performed using the *md_analyze* and *md_analyzeres* macros to obtain RMSD-Cα atoms (Root Mean Square Deviation-Cα atoms), RMSF (Root Mean Square Fluctuation), R_g (Radius of Gyration), SASA (Solvent Accessible Surface Area), and solute H-bond values [24–26]. The MD simulation data were generated after accounting for the equilibration conditions defined in the macro file. The MD simulation data were generated under CPU and GPU-based computational performance.

2.7. Calculation of binding energy using MM-PBSA.

Binding energy calculations using the Molecular Mechanics Poisson-Boltzmann Surface Area (MM-PBSA) were applied using the *md_analyzebindenergy* macro. In this setup, the AMBER14 force field was again applied, and the MM-PBSA calculation results are presented in kJ/mol. A higher binding energyndicates stronger binding between the ligand and receptor, suggesting a more favorable interaction [24–26].

2.8. Principal component analysis (PCA) and dynamic cross-correlation matrix (DCCM).

PCA and DCCM analyses of the 300 ns MD simulation data were conducted using R Studio (Version 4.4.2) with the Bio3D package. The function used to perform PCA was "mktrj.pca", whereas the "dccm" function was employed to compute the DCCM.

3. Results and Discussion

Here, we conducted computational *in silico* research to identify phytochemical compounds in *C. variegatum* as potential new anticancer agents targeting Bcl-2. In an effort to identify and propose new drug candidates for cancer, Bcl-2 is a promising target because it is an important regulator of apoptosis (programmed cell death), a fundamental biological process that is regulated byhe formation of heterodimers with selective pro-apoptotic members of the Bcl-2 family [8]. We chose *C. variegatum* because several studies have successfully tested spirale (SCE) cultivars of C. variegatum on three cancer cell lines (MCF-7, HepG2, and HeLa) and report promising results [27]. Aside from that research, to our knowledge, no study has used the phytochemical compounds in *C. variegatum* specifically as anticancer agents targeting Bcl-2. However, a research report examining *C. variegatum* Zanzibar (Pictum spot) as an inhibitor of tumor activity (antitumor) also showed promising results [28]. *C. variegatum* is commonly used in Traditional Chinese Medicine (TCM) and is known for its various medicinal benefits and effects [5]. In this study, we used a computational *in silico* approach that included molecular docking, ADME, DFT studies, molecular dynamics, and advanced PCA and DCCM analysis. Molecular docking and ADME were combined to support the initial screening phase of drug discovery using *in silico* methods.

3.1. Molecular docking.

Based on molecular docking results identifying phytochemical compounds in *C. variegatum* as potential Bcl-2 protein inhibitors, the findings are presented in Table 1. Venetoclax, the control drug, ranked first in terms of binding energy.

Table 1. The binding energy data were evaluated in kcal/mol using YASARA structure.

Rank	CID	Compound	Binding energy (kcal/mol)
1	49846579	Venetoclax (Control)	10.598
2	92097	Taraxerol	8.868
3	73170	α- amyrin	8.346
4	1794427	Chlorogenic acid	8.317
5	10494	Caryophylline	8.282
6	5280441	Vitexin	7.847
7	5280805	Rutin	7.787
8	5281855	Ellagic acid	7.447
9	72276	Epicatechin	7.447
10	5280443	Apigenin	7.223
11	5281675	Orientin	7.084
12	442664	Vicenin	7.014
13	689043	Caffeic acid	6.401
14	637542	p-Coumaric acid	6.358
15	16754	Glaucine	6.271
16	445858	Ferulic acid	6.174
17	8468	Vanillic acid	5.62
18	985	Hexadecanoic acid	4.542

This was followed by the investigated ligand taraxerol, which exhibited the highest binding energy (in kcal/mol, with more positive values indicating stronger binding) among all

investigated ligands. Therefore, both venetoclax and the top-scoring test ligand taraxerol were selected for further analysis to evaluate their ADME properties.

3.2. ADME analysis.

To assess the ADME characteristics, we utilized SwissADME, and the results are presented in Table 2. SwissADME predictions indicated that venetoclax does not comply with Lipinski's Rule of Five, suggesting limited suitability for oral bioavailability. In addition, the control compounds were characterized by relatively high molecular weights (g/mol). In contrast, the top-ranked test ligand, taraxerol, satisfied all Lipinski criteria for oral administration, highlighting its drug-like properties and potential as an orally viable candidate.

Table 2. ADME analysis of the control drug and top-scoring test ligand.

Compound	Molecular weight (g/mol)	TPSA (Å²)	Lipinski	Synthetic accessibility
Venetoclax	868.44	183.09	No; 2 violations: MW>500, NorO>10	6.05
Taraxerol	426.72	20.23	Yes; 1 violation: MLOGP>4.15	6.04

Molecular docking is a widely used approach to support drug discovery. In this study, taraxerol, which showed a binding energy value close to that of venetoclax, showed promising results and is a potential inhibitor candidate for Bcl-2. Additionally, the Lipinski rule applied to taraxerol, with no violations, suggests that it meets important criteria in compound screening and evaluating its suitability as a drug (drug-likeness). Moreover, Lipinski assessed the likelihood that a chemical compound would become an oral drug in humans. This stage serves as the initial screening phase based on predictions. Lipinski is associated with molecular propertiesmportant for the pharmacokinetics of drugs in the human body, commonly referred to as ADME [29].

The ADME profile plays a decisive role in determining a compound's translational potential, as many otherwise promising drug candidates ultimately fail due to suboptimal pharmacokinetic behavior, including poor absorption, limited systemic distribution, rapid metabolic degradation, or inefficient elimination. These limitations, together with toxicity-related risks, often emerge late in development and result in substantial financial losses. Consequently, early-stage ADMET screening has become a critical strategy for identifying compounds with inherent pharmacokinetic liabilities before costly preclinical and clinical investments are made. Another important aspect is the necessity to exclude pan-assay interference compounds (PAINS), which frequently generate misleading bioactivity signals and divert research efforts. Although natural products offer exceptional structural diversity and valuable physicochemical properties, their pharmacokinetic profiles remain highly variable and may not always meet established drug-likeness criteria. For this reason, a more explicit discussion of potential pharmacokinetic constraints, along with the urgency of integrating comprehensive ADME data, is essential to provide a balanced and informative evaluation of each candidate's drug development viability [30].

3.3. Post-docking analysis.

Protein–ligand (receptor-ligand) interactions were analyzed and visualized using Discovery Studio. Venetoclax, a co-crystallized ligand, exhibited van der Waals, conventional hydrogen, carbon-hydrogen, alkyl, and π-alkyl interactions. It forms hydrophobic interactions with six amino acid residues: Ala149, Leu137, Phe104, Tyr108, Met115, and Phe153.

Additionally, hydrogen bonds were observed between Venetoclax and three amino acid residues of Bcl-2: Ala100, Asp103, and Gly145. These interactions occur within the binding site region of the Bcl-2 receptor. Taraxerol, identified as the top test ligand, exhibits van der Waals, alkyl, and π-alkyl interactions. Specifically, taraxerol formed alkyl interactions with Met115, Leu137, and Ala149, and a π-alkyl interaction with Phe104. Notably, taraxerol shared a common interaction site with venetoclax, namely Met115, where both ligands engaged in hydrophobic interactions. This overlap suggests that taraxerol may inhibit Bcl-2 through a similar binding mechanism (Figure 2).

The interaction we highlighted is Met115, where both complexes, Bcl-2-Venetoclax and Bcl-2-Taraxerol, interact hydrophobically with amino acid residues within the binding site. This interaction contributes to the stability of the protein-ligand complex [31,32]. We performed docking by preparing the ligands using the semi-empirical QM-AM1 method, as this method is specifically designed to calculate enthalpies of formation for chemical systems. AM1 is widely used in enthalpy-*of*-formation calculations and has become a standard tool for organic chemists, both theoretically and experimentally [33].

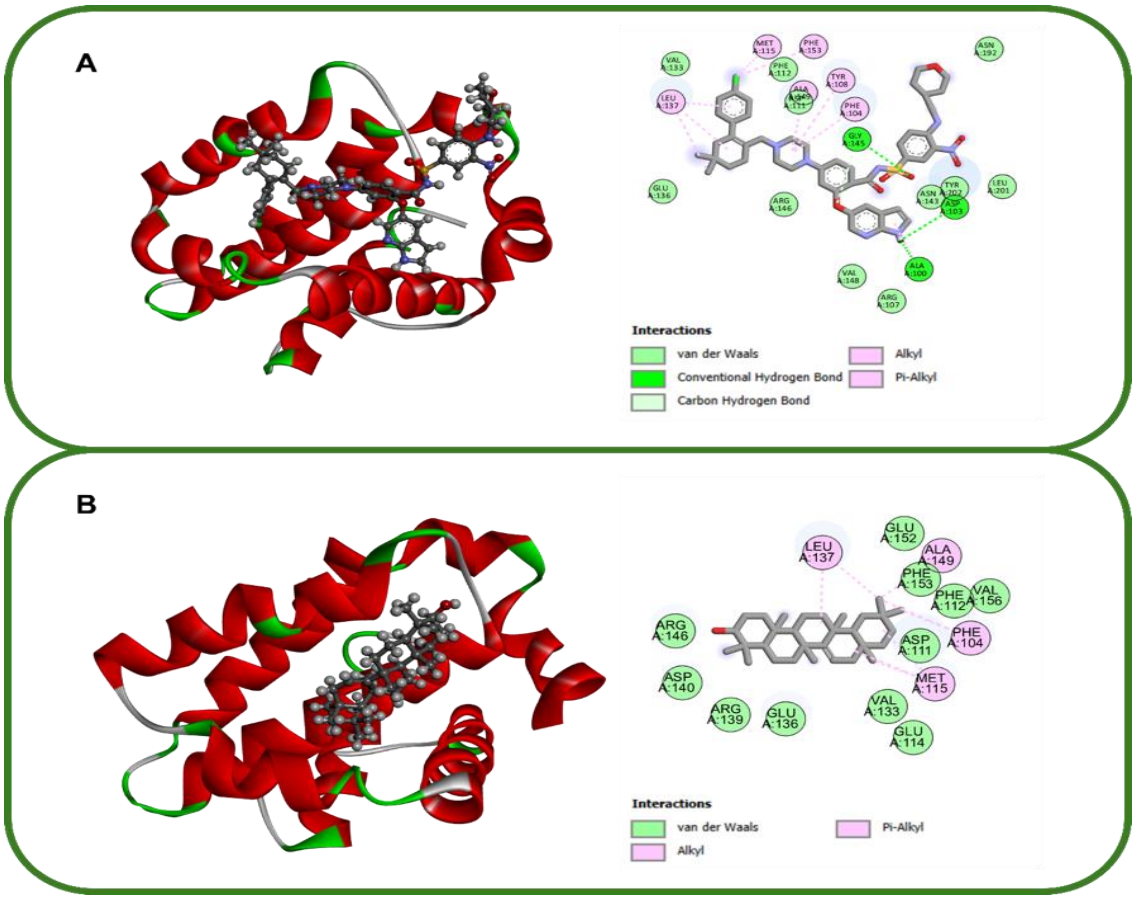

Figure 2. Receptor-ligand interactions. **(a)** Bcl 2-Venetoclax; **(b)** Bcl 2-Taraxerol.

3.4. DFT analysis.

Density functional theory (DFT) calculations were performed to characterize the electronic properties of taraxerol by evaluating the energies of its frontier molecular orbitals (FMOs), including the HOMO and LUMO. Venetoclax was used as the reference. As shown in Figure 3, Venetoclax exhibits HOMO and LUMO energies of –0.1802 eV and –0.1285 eV, respectively, whereas taraxerol exhibits HOMO and LUMO energies of –0.199 eV and –0.0185

eV, respectively. The corresponding HOMO–LUMO energy gaps were –0.0517 eV for venetoclax and –0.1805 eV for taraxerol.

It is important to note that the HOMO–LUMO gap does not directly quantify molecular "stability" in an absolute sense, but rather reflects electronic excitation characteristics, chemical hardness/softness, and the ease of charge transfer. Molecules with narrower gaps are typically more chemically reactive or electronically polarizable, whereas molecules with wider gaps exhibit greater chemical hardness and a lower propensity for intramolecular charge redistribution. Based on this interpretation, taraxerol's larger HOMO–LUMO gap suggests a comparatively harder electronic structure, whereas venetoclax's smaller gap indicates a more electronically responsive or chemically softer profile [34]. The DFT-optimized geometry of taraxerol (def2-SVP basis set) provides additional insight into its electronic distribution, but these FMO-derived parameters should be understood as descriptors of reactivity, charge-transfer behavior, and potential interaction modes with biological targets, rather than as standalone indicators of thermodynamic stability. Consistent with previous anticancer-related DFT studies [35,36], the FMO analysis presented here is intended to support early-stage structure–activity reasoning and to complement subsequent molecular docking and MD-based analyses [36,37].

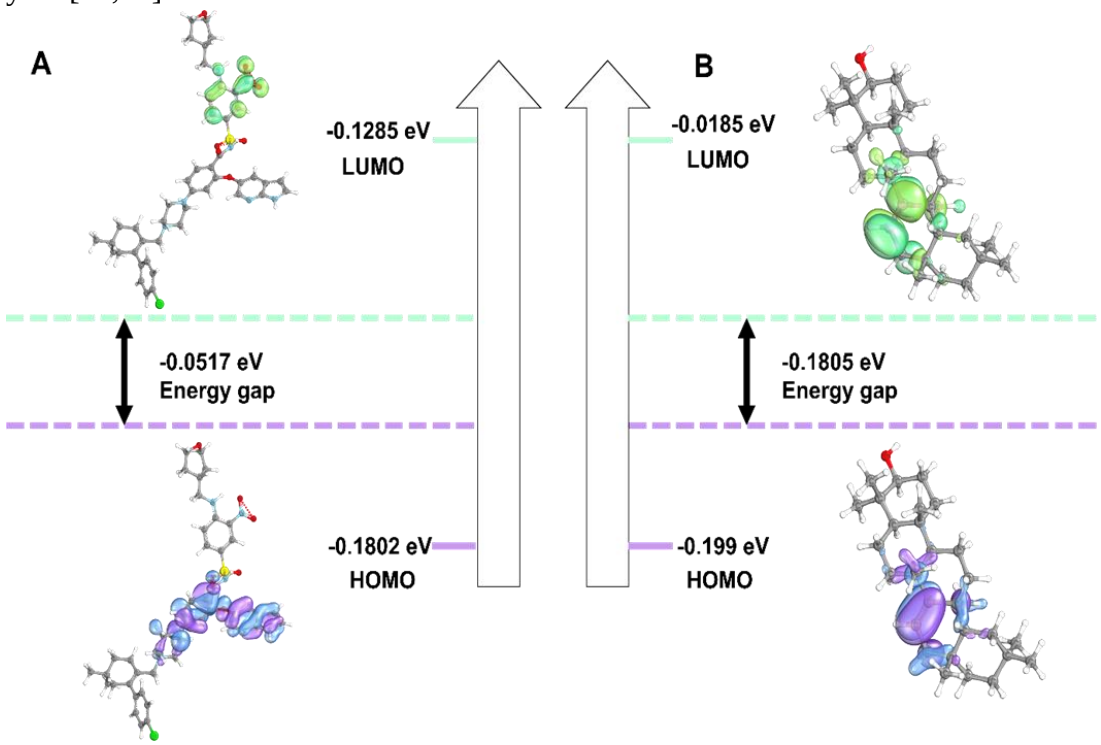

Figure 3. HOMO, LUMO, and Energy Gap values. **(a)** Venetoclax; **(b)** Taraxerol.

3.5. Post-MD analysis.

Next, we performed MD simulations to evaluate the structural stability of the Bcl-2 ligand complexes throughout the 300 ns trajectory. As shown in Figure 4A, both ligand systems displayed RMSDCα profiles indicative of stable conformational behavior. The Bcl-2–Taraxerol complex reached equilibrium earlier in the trajectory and maintained an average RMSDCα value of 2.042 Å, whereas the Bcl-2–Venetoclax complex exhibited slightly lower fluctuations, with an average RMSDCα of 1.705 Å. Although these numerical differences are modest, they suggest that venetoclax stabilizes the Bcl-2 backbone more effectively than taraxerol. Importantly, the overall RMSD trends for both complexes remained within the range

commonly observed for table protein–ligand systems in long-timescale MD simulations [37]. This indicates that the Cα atoms preserve their structural integrity across the trajectory, with taraxerol inducing only marginally greater backbone mobility than the reference ligand.

To characterize residue-level flexibility within the Bcl-2 binding pocket, RMSF analysis was performed for all amino acid residues (Figure 4B). Particular attention was given to Met115, a hydrophobic anchor residue that plays a central role in stabilizing both venetoclax and taraxerol. The RMSF values at Met115 were 1.503 Å for venetoclax and slightly lower for taraxerol at 1.41 Å. Although the numerical difference is modest, the consistently lower fluctuations observed for taraxerol indicate more restricted local mobility at this hotspot, which may help maintain hydrophobic contacts essential for complex stabilization. Overall, the RMSF profiles of both complexes showed a similar distribution of flexible and rigid regions, consistent with the global stability trends observed in the RMSD analysis. However, the slightly reduced flexibility around Met115 in the taraxerol complex suggests a comparable, if not marginally enhanced, local stabilization relative to venetoclax, consistent with previous reports linking lower residue fluctuations toore persistent ligand–receptor interactions [38].

The structural compactness of Bcl-2 was further evaluated using the radius of gyration (R_g), as shown in Figure 4C. Over the 300 ns simulation, the highest R_g value was observed in the Bcl-2–Venetoclax complex at 14.923 Å, while the Bcl-2–Taraxerol complex reached a maximum of 15.225 Å at 289.75 ns. The average R_g values were 14.686 and 14.745 Å for the venetoclax and taraxerol complexes, respectively, with a marginal difference of 0.059 Å.

Figure 4D presents the SASA profiles over 300 ns to evaluate the changes in the Bcl-2 surface due to structural shrinkage or expansion. The average SASA values were 7491.644 Å^2 for the Bcl-2–Venetoclax complex and 7503.393 Å^2 for the Bcl-2–Taraxerol complex, suggesting that taraxerol induced a greater surface area alteration in Bcl-2.

In this study, protein folding was also assessed through the number of internal hydrogen bonds (H-bonds), as illustrated in Figure 4E. The highest H-bond production occurred at the beginning of the simulation in the Bcl-2–taraxerol complex, with a peak of 141 bonds. At the end of the 300 ns simulation, the average number of H-bonds was 118.151 for the Bcl-2–Taraxerol complex and 118.53 for Bcl-2–Venetoclax. Despite a slightly lower average, the taraxerol complex showed higher initial H-bond formation.

A strong correlation was observed between higher H-bond formation and improved binding energy throughout the simulation. The binding energy was calculated using the Molecular Mechanics Poisson-Boltzmann Surface Area (MM-PBSA) method. Taraxerol showed a favorable interaction with Bcl-2, with an average binding energy of 303.235 kJ/mol, which was higher than that of venetoclax, suggesting a stronger binding. Moreover, the increased H-bond production contributed to stronger, more stable interactions, as evidenced by the more positive binding energies.

In this study, we performed MD simulations on Bcl-2–Venetoclax and Bcl-2–Taraxerol complexes. MD enabled us to comprehensively assess the molecular dynamics of biological systems and conformational changes of the complexes. Numerous studies have employed MD simulations as part of efforts to discover new drug candidates. The combination of molecular docking and MD is a highly recommended approach, considering that docking is a static method; therefore, MD simulations were conducted to understand better dynamic aspects such as receptor flexibility and structural alterations in a study, Almansour *et al*. [39], searching for inhibitor Bcl-2 from Natural Product Atlas (NPAtlas) by using the combination of docking and MD. There is an advanced distinction in this study, as previous studies only used a 200 ns

trajectory, whereas our research applied a 300 ns trajectory. This trajectory defines the numerical integration of the equations of motion for interacting atomic systems over a specific timeframe. MD provides detailed data based on the motion of the system. Nevertheless, through the 300 ns trajectory in our study, we revealed a correlation between hydrogen bond (H-bond) production and stability, as evidenced by the favorable binding energy calculated using MM-PBSA. MM-PBSA has been widely used to calculate binding energy, as implemented in YASARA, where a more positive binding energy value indicates more favorable binding [40]. The averaged values from the 300-ns trajectory that was generated and evaluated are presented in Table 3.

Table 3. The averaged data were obtained from the evaluated 300-ns trajectory.

Ligand	RMSDCα	RMSF	Rg	SASA	Solute H-bond	Binding energy via MM-PBSA
Venetoclax	1.705	1.387	14.686	7491.644	118.53	291.115
Taraxerol	2.042	1.429	14.745	7503.393	118.151	303.235

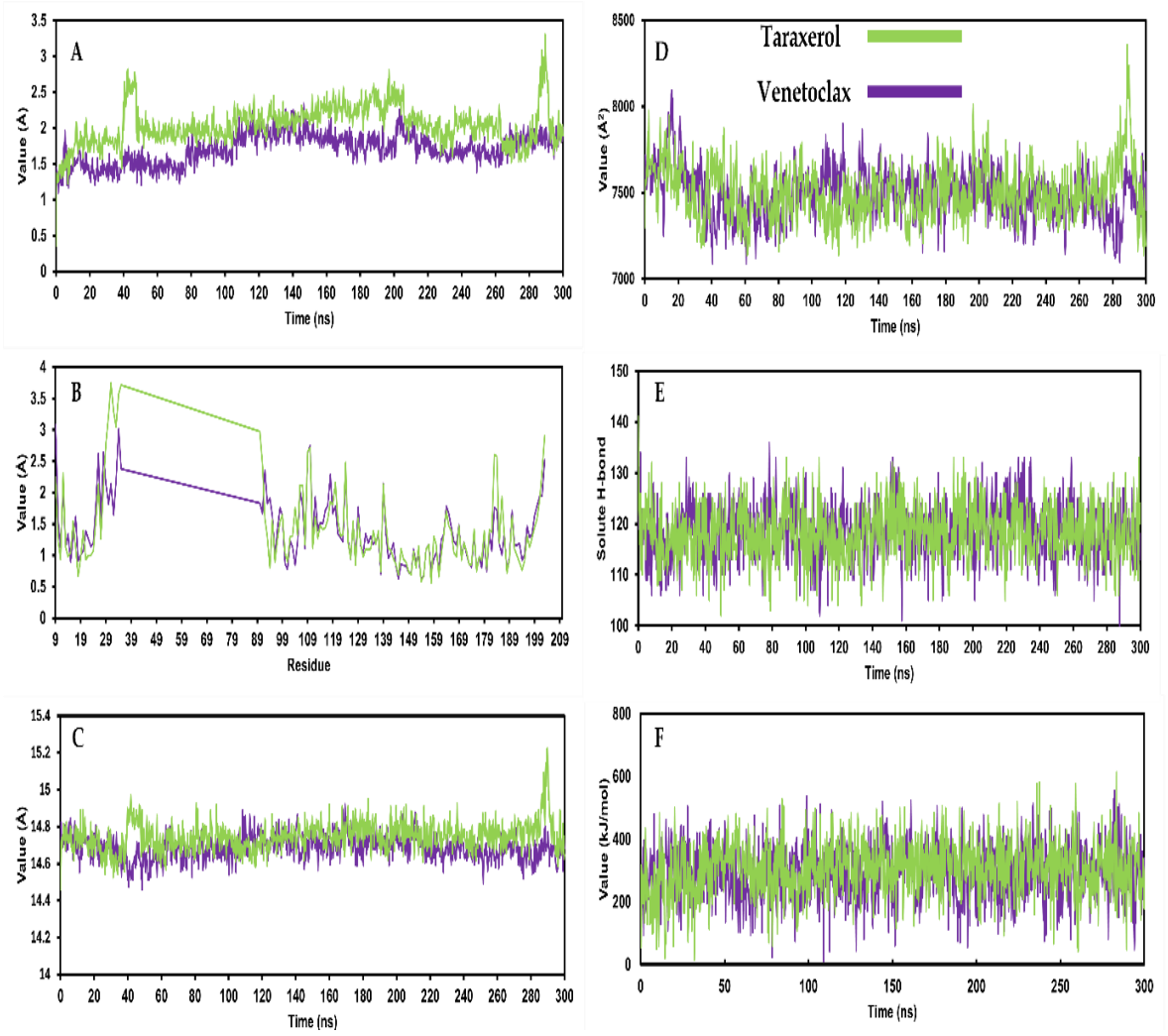

Figure 4. Evaluation of MD simulation parameters with a 300 ns trajectory. **(a)** Root Mean Square Deviation-Cα atoms RMSDCα; **(b)** Root Mean Square Fluctuation (RMSF); **(c)** Radius of Gyration (R_g); **(d)** Solvent Accessible Surface Area (SASA); **(e)** Solute hydrogen bonding (H-bond); **(f)** Binding energy via the Molecular Mechanics Poisson-Boltzmann Surface Area (MM-PBSA).

3.6. PCA and DCCM analysis.

The big data produced from the 300 ns MD simulation was then analyzed using PCA. PCA helped us reduce and visualize the protein-ligand (receptor-ligand) complex's movement

over 300 ns, as shown in Figure 5. Figure 5A shows the PCA of the Bcl 2-Venetoclax complex, where the values of PC1, PC2, and PC3 were 22.76%, 8.95%, and 7.26%, respectively. For the Bcl 2-Taraxerol complex, the values of PC1, PC2, and PC3 were 23.2%, 12.22%, and 6.37%, respectively (Figure 5B). To understand the Bcl-2 conformation in relation to positive and negative correlations, we calculated it using DCCM. Figure 5C shows the DCCM plot of the Bcl-2-Venetoclax complex, with a concentration of red color in the plot. Similarly, Figure 5D shows the DCCM plot of the Bcl 2-Taraxerol complex, where the red color concentration is similar to that of the Bcl 2-Venetoclax complex. The presence of the red color concentration in the DCCM plot indicates stability.

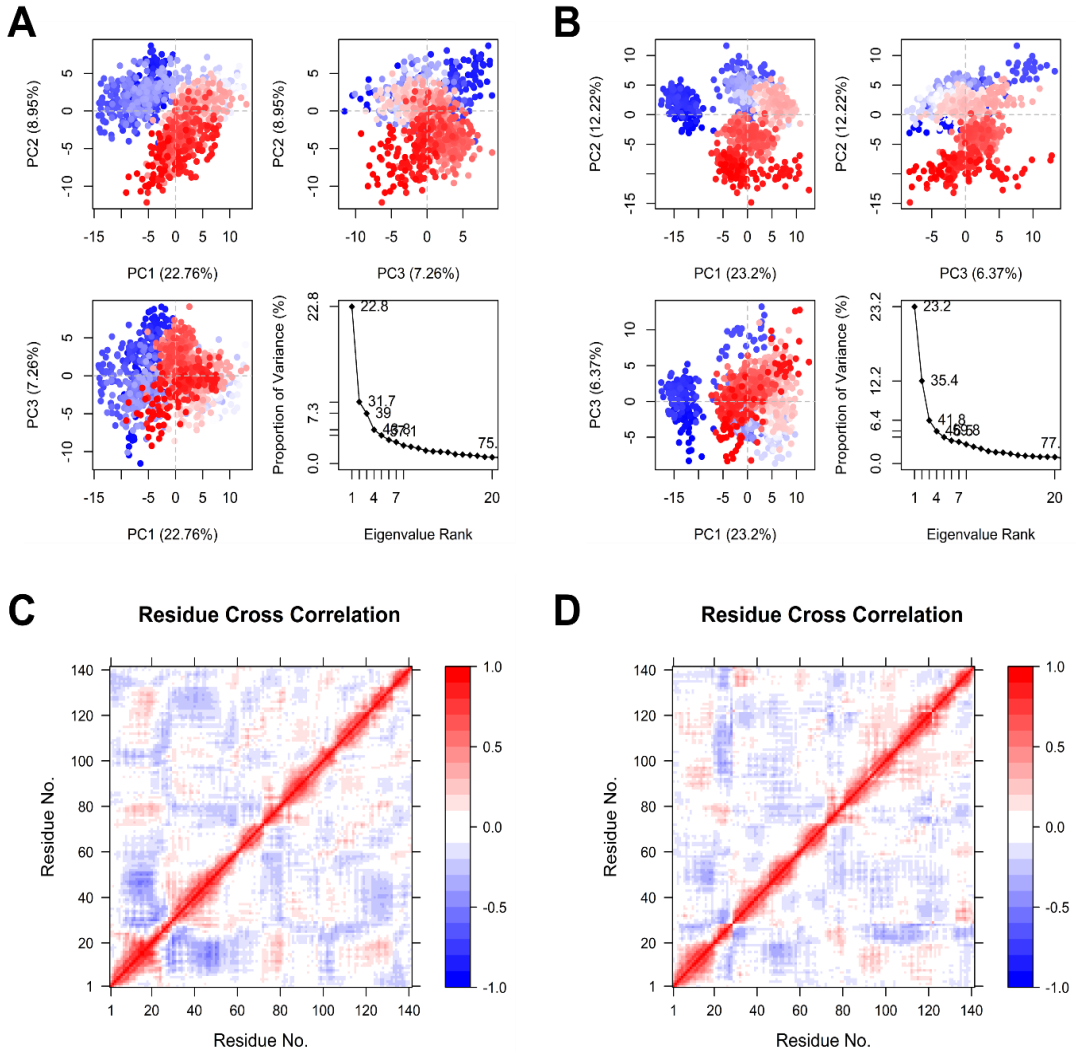

Figure 5. Principal component analysis and dynamic cross-correlation matrix of the protein-ligand complex based on big data from a 300 ns MD simulation. **(a)** The PCA data for the Bcl 2-Venetoclax complex; **(b)** The PCA data for the Bcl 2- Taraxerol complex; **(c)** The DCCM data for the Bcl 2-Venetoclax complex; **(d)** The DCCM data for the Bcl 2-Taraxerol complex. Each plot indicates the combination of the top three eigenvalues, namely PC1-PC2, PC2-PC3, and PC2-PC3. Additionally, there is a cumulative plot of eigenvalues against the percentage variance (PCA Analysis). Colors indicate parallel and antiparallel conformations, depicted with color gradients from blue to red, showing the movement of the Cα atoms during the MDS (DCCM Analysis).

The 300 ns MD simulation big data were then mapped and visualized using PCA and DCCM. PCA is a statistical method used to analyze the variation and motion patterns within the data. In the context of 300 ns MD simulation big data, PCA is used to interpret the data in order to understand complexities such as collective motions, determine variability, and identify conformational state changes in the protein structure over the course of the simulation

trajectory [41,42], Meanwhile, DCCM was calculated based on the 300 ns MD simulation trajectory to analyze the correlation of movements between atoms or residues within the protein. Based on the DCCM plot, we observed that the motion characteristics of the Bcl-2–Taraxerol complex showed a dense red coloration, indicating a strong correlation, similar to the DCCM plot of the Bcl-2–Venetoclax complex.

This study was limited by its reliance on *in silico* computational methods as the primary approach. As a prediction-based technique, *in silico* analysis requires further validation to confirm the inhibitory activity of the phytochemical compounds from *C. variegatum*, particularly the predicted efficacy of taraxerol in targeting Bcl-2, through both *in vitro* and *in vivo* experiments. On the other hand, the strength of this research lies in the use of advanced MD simulations extending to 300 ns. This trajectory represents a form of big data analysis, interpreted through PCA and DCCM, to support the identification of Taraxerol as a promising inhibitor candidate based on *in silico* predictions.

4. Conclusions

Based on the results of this study, we successfully proposed a potential Bcl-2 inhibitor candidate as a novel anticancer agent using a computational *in silico* approach. This result was obtained through molecular docking screening, which showed that the binding energy of taraxerol was close to that of venetoclax, with a difference of 1.73 kcal/mol. In the context of this study, a more positive (i.e., higher) binding energy value indicates a stronger interaction between the ligand and the target protein. Moreover, taraxerol fulfilled the drug-likeness criteria based on ADME prediction using Lipinski's Rule of Five. Our DFT calculations also indicated that taraxerol has good molecular stability. MD simulations yielded favorable binding energies via MM-PBSA calculations, confirming stable interactions with Bcl-2 and similarities in PCA characteristics and DCCM plots between the Bcl-2–Taraxerol and Bcl-2–Venetoclax complexes. Nevertheless, this study represents an early stage in the anticancer drug discovery process. Further investigations are required, including laboratory-based evaluations, ranging from *in vitro* assays to *in vivo* validation using appropriate animal models.

Author Contributions

Conceptualization, W.N., G.M.G., M.A.D., and Y.A.; methodology, W.N., G.M.G., M.A.D., and D.A.,; software, G.M.G., M.A.D., Y.A., and I.M.A; validation, W.N., G.M.G., M.A.D., E.S.S., F.S., Y.A., D.A., and I.M.A.; formal analysis, W.N., G.M.G., M.A.D., E.S.S., F.S., Y.A., D.A., and I.M.A.; investigation, G.M.G. and M.A.D ; resources, W.N., G.M.G., M.A.D., E.S.S., F.S., Y.A., D.A., and I.M.A.; data curation, W.N., G.M.G., M.A.D., E.S.S., F.S., Y.A., D.A., and I.M.A.; writing—original draft preparation, G.M.G. and M.A.D.; writing—review and editing, W.N., E.S.S., F.S., Y.A., D.A., and I.M.A.; visualization, G.M.G. and M.A.D.; supervision, W.N., E.S.S., F.S., Y.A., D.A., and I.M.A.; project administration, W.N.; funding acquisition, W.N.. All authors have read and agreed to the published version of the manuscript.

Institutional Review Board Statement

Not applicable.

Informed Consent Statement

Not applicable.

Data Availability Statement

Data supporting the findings of this study are available upon reasonable request from the corresponding author.

Funding

This research received no external funding.

Acknowledgments

This research has no acknowledgments.

Conflicts of Interest

The authors declare no conflict of interest.

References

1. Liu, B.; Zhou, H.; Tan, L.; Siu, K.T.H.; Guan, X.-Y. Exploring treatment options in cancer: tumor treatment strategies. *Signal Transduct. Target. Ther.* **2024**, *9*, 175, https://doi.org/10.1038/s41392-024-01856-7.
2. Cao, Y.; DePinho, R.A.; Ernst, M.; Vousden, K. Cancer research: past, present and future. *Nat. Rev. Cancer* **2011**, *11*, 749-754, https://doi.org/10.1038/nrc3138.
3. Hasim, H.; Kurniawati, S.O.; Priosoeryanto, B.P.; Faridah, D.N.; Puspita, R. Antiproliferation activity of God's crown fruit (Phaleria macrocarpa) extract and fractions against MCM-B2 breast cancer cells. *J. Appl. Pharm. Sci.* **2020**, *10*, 052-058, https://doi.org/10.7324/JAPS.2020.103006.
4. Hafezi, S.; Rahmani, M. Targeting BCL-2 in Cancer: Advances, Challenges, and Perspectives. *Cancers* **2021**, *13*, 1292, https://doi.org/10.3390/cancers13061292.
5. Pandey, S.; Singh, S. Exploring phytoconstituents and pharmacological profile of *Codiaeum variegatum* (L.), Garden croton. *Pharmacol. Res. - Mod. Chin. Med.* **2023**, *9*, 100327, https://doi.org/10.1016/j.prmcm.2023.100327.
6. Lv, X.; Jiang, Y.; Wang, X.; Xie, H.; Dou, G.; Wang, J.; Yang, W.; Wang, H.; Li, Z.; Zhang, X.; Chen, Z. Computational study on novel natural inhibitors targeting BCL2. *Med. Oncol.* **2021**, *38*, 94, https://doi.org/10.1007/s12032-021-01513-x.
7. Othman, B.; Beigh, S.; Albanghali, M.A.; Sindi, A.A.A.; Shanawaz, M.A.; Ibahim, M.A.E.M.; Marghani, D.; Kofiah, Y.; Iqbal, N.; Rashid, H. Comprehensive pharmacokinetic profiling and molecular docking analysis of natural bioactive compounds targeting oncogenic biomarkers in breast cancer. *Sci. Rep.* **2025**, *15*, 5426, https://doi.org/10.1038/s41598-024-84401-4.
8. Gowtham, H.G.; Ahmed, F.; Anandan, S.; Shivakumara, C.S.; Bilagi, A.; Pradeep, S.; Shivamallu, C.; Shati, A.A.; Alfaifi, M.Y.; Elbehairi, S.E.I.; Achar, R.R.; Silina, E.; Stupin, V.; Murali, M.; Kollur, S.P. *In Silico* Computational Studies of Bioactive Secondary Metabolites from *Wedelia trilobata* against Anti-Apoptotic B-Cell Lymphoma-2 (Bcl-2) Protein Associated with Cancer Cell Survival and Resistance. *Molecules* **2023**, *28*, 1588, https://doi.org/10.3390/molecules28041588.
9. Ghosh, S.; Basu, S.; Kayal, T.; Ashok, G.; Ramaiah, S.; Anbarasu, A. Computational advancements to facilitate therapeutic application of phytochemicals: Where do we stand?. *Discov. Appl. Sci.* **2025**, *7*, 491, https://doi.org/10.1007/s42452-025-06772-1.
10. Hashemi, S.M.J.; Ghalehnoei, H.; Barzegar, A.; Feizi-Dehnayebi, M.; Akhtari, J.; Mellati, A. In silico discovery of multi-target small molecules and efficient siRNA design to overcome drug resistance in breast cancer via local therapy. *J. Mol. Graph. Model.* **2025**, *140*, 109086, https://doi.org/10.1016/j.jmgm.2025.109086.
11. Cavalcante, B.R.R.; Freitas, R.D.; Siquara da Rocha, L.d.O.; Santos, R.d.S.B.D.; Souza, B.S.d.F.; Ramos, P.I.P.; Rocha, G.V.; Gurgel Rocha, C.A. *In silico* approaches for drug repurposing in oncology: a scoping review. *Front. Pharmacol.* **2024**, *15*, 1400029, https://doi.org/10.3389/fphar.2024.1400029.

12. Jain, N.K.; Chandrasekaran, B.; Khazaleh, N.; Jain, H.K.; Lal, M.; Joshi, G.; Jha, V. Computational Network Pharmacology, Molecular Docking, and Molecular Dynamics to Decipher Natural Compounds of *Alchornea laxiflora* for Liver Cancer Chemotherapy. *Pharmaceuticals* **2025**, *18*, 508, https://doi.org/10.3390/ph18040508.
13. Arango, J.P.B.; Rodriguez, D.Y.M.; Cruz, S.L.; Ocampo, G.T. *In silico* evaluation of pharmacokinetic properties and molecular docking for the identification of potential anticancer compounds. *Comput. Biol. Chem.* **2026**, *120*, 108626, https://doi.org/10.1016/j.compbiolchem.2025.108626.
14. Birkinshaw, R.W.; Gong, J.-n.; Luo, C.S.; Lio, D.; White, C.A.; Anderson, M.A.; Blombery, P.; Lessene, G.; Majewski, I.J.; Thijssen, R.; Roberts, A.W.; Huang, D.C.S.; Colman, P.M.; Czabotar, P.E. Structures of BCL-2 in complex with venetoclax reveal the molecular basis of resistance mutations. *Nat. Commun.* **2019**, *10*, 2385, https://doi.org/10.1038/s41467-019-10363-1.
15. Piotto, S.; Sessa, L.; Iannelli, P.; Concilio, S. Computational study on human sphingomyelin synthase 1 (hSMS1). *Biochim. Biophys. Acta-Biomembr.* **2017**, *1859*, 1517-1525, https://doi.org/10.1016/j.bbamem.2017.04.004.
16. Land, H.; Humble, M.S. YASARA: A Tool to Obtain Structural Guidance in Biocatalytic Investigations. In Protein Engineering: Methods and Protocols; Bornscheuer, U.T., Höhne, M., Eds.; Springer New York: New York, NY, **2018**; Volume 1685, pp. 43-67, https://doi.org/10.1007/978-1-4939-7366-8_4.
17. Nursyarah, A.T.; Safithri, M.; Andrianto, D. Red Betel Leaf Bioactive Compounds as ERα Receptor Inhibitors In Silico and MCF-7 Cell Anticancer In Vitro. *HAYATI J. Biosci.* **2023**, *30*, 789-796, https://doi.org/10.4308/hjb.30.5.789-796.
18. Umar, M.; Safithri, M.; Pratama, R. In Silico Study of Anticancer Activity of Red Betel Leaves Bioactive Compounds against Colon Cancer Marker Proteins. *HAYATI J. Biosci.* **2022**, *30*, 113-121, https://doi.org/10.4308/hjb.30.1.113-121.
19. Daina, A.; Michielin, O.; Zoete, V. SwissADME: a free web tool to evaluate pharmacokinetics, drug-likeness and medicinal chemistry friendliness of small molecules. *Sci. Rep.* **2017**, *7*, 42717, https://doi.org/10.1038/srep42717.
20. Manicum, A.-L.E.; Louis, H.; Mathias, G.E.; Agwamba, E.C.; Malan, F.P.; Unimuke, T.O.; Nzondomyo, W.J.; Sithole, S.A.; Biswas, S.; Prince, S. Single crystal investigation, spectroscopic, DFT studies, and *in-silico* molecular docking of the anticancer activities of acetylacetone coordinated Re(I) tricarbonyl complexes. *Inorg. Chim. Acta* **2023**, *546*, 121335, https://doi.org/10.1016/j.ica.2022.121335.
21. Gupta, A.K.; Vaishnav, Y.; Jain, S.K.; Annadurai, S.; Kumar, N. Exploring novel Apalutamide analogues as potential therapeutics for prostate cancer: design, molecular docking investigations and molecular dynamics simulation. *Front. Chem.* **2024**, *12*, 1418975, https://doi.org/10.3389/fchem.2024.1418975.
22. Truong, D.T.; Ho, K.; Thai, C.T.; Do Thi Mai, D.; Tam, N.M.; Phung, V.B.T.; Nguyen, M.T. Molecular dynamics simulations reveal a strong binding capacity of colossolactone H to the EGFR inactive conformation. *Phys. Chem. Chem. Phys.* **2025**, *27*, 13845-13860, https://doi.org/10.1039/D5CP00817D.
23. Mazri, R.; Ouassaf, M.; Zekri, A.; Khan, S.U.; Rengasamy, K.R.R.; Alhatlani, B.Y. In Silico Network Pharmacology, Molecular Docking, and Molecular Dynamics Analysis of Rosemary-Derived Compounds as Potential HSP90 Inhibitors for Cancer Therapy. *Curr. Issues Mol. Biol.* **2025**, *47*, 860, https://doi.org/10.3390/cimb47100860.
24. Krieger, E.; Vriend, G. YASARA View—molecular graphics for all devices—from smartphones to workstations. *Bioinformatics* **2014**, *30*, 2981–2982, https://doi.org/10.1093/bioinformatics/btu426.
25. Krieger, E.; Vriend, G. New ways to boost molecular dynamics simulations. *J. Comput. Chem.* **2015**, *36*, 996–1007, https://doi.org/10.1002/jcc.23899.
26. Krieger, E.; Koraimann, G.; Vriend, G. Increasing the precision of comparative models with YASARA NOVA—a self-parameterizing force field. *Proteins. Struct., Funct., Bioinf.* **2002**, *47*, 393–402, https://doi.org/10.1002/prot.10104.
27. Suphiratwanich, P.; Buranrat, B.; Boontha, S. Anti-cancer effects of the extracts of broad and spirale cultivars of *Codiaeum variegatum* (L.) Blume on MCF-7, HepG2, and HeLa cell lines. *J. Herbmed Pharmacol.* **2023**, *12*, 512–520, https://doi.org/10.34172/jhp.2023.45002.
28. Rashwan, R.T.; Moustafa, A.M.Y.; Taie, H.A.A.; Marzouk, M. Codiaeum variegatum Zanzibar (Pictum spot): LC-MS/MS Phytochemical Profile and In vitro Antioxidant and Antitumor Activities. *Egypt. J. Chem.* **2024**, *67*, 339-357, https://doi.org/10.21608/ejchem.2024.259570.9125.
29. Husnawati, H.; Kusmardi, K.; Kurniasih, R.; Hasan, A.Z.; Andrianto, D.; Julistiono, H.; Priosoeryanto, B.P.; Artika, I.M.; Salleh, M.N. Investigation of Chemical Compounds from Phomopsis Extract as Anti-Breast Cancer Using LC-MS/MS Analysis, Molecular Docking, and Molecular Dynamic Simulations. *Int. J. Technol.* **2023**, *14*, 1476-1486, https://doi.org/10.14716/ijtech.v14i7.6696.
30. Ancuceanu, R.; Lascu, B.E.; Drăgănescu, D.; Dinu, M. In Silico ADME Methods Used in the Evaluation of Natural Products. *Pharmaceutics* **2025**, *17*, 1002, https://doi.org/10.3390/pharmaceutics17081002.
31. Tondar, A.; Sánchez-Herrero, S.; Bepari, A.K.; Bahmani, A.; Calvet Liñán, L.; Hervás-Marín, D. Virtual Screening of Small Molecules Targeting BCL2 with Machine Learning, Molecular Docking, and MD Simulation. *Biomolecules* **2024**, *14*, 544, https://doi.org/10.3390/biom14050544.

32. Warnasih, S.; Mulyati, A.H.; Widiastuti, D.; Zahra, A.C.; Sugita, P.; Ambarsari, L.; Dianhar, H.; Rahayu, D.U.C. Anticancer Potency of Methanol Extract from Terminalia catappa Leaves Using In Vitro and In Silico Methods. *Trends Sci.* **2024**, *21*, 8057, https://doi.org/10.48048/tis.2024.8057.
33. Klein, E.; Matis, M.; Lukeš, V.; Cibulková, Z. The applicability of AM1 and PM3 semi-empirical methods for the study of N–H bond dissociation enthalpies and ionisation potentials of amine type antioxidants. *Polym. Degrad. Stab.* **2006**, *91*, 262-270, https://doi.org/10.1016/j.polymdegradstab.2005.05.010.
34. Jayavel, P.; Ramasamy, V.; Amaladoss, N.; Renganathan, V.; Shupeniuk, V.I. A facile synthesis, characterization, DFT, ADMET and *in-silico* molecular docking analysis of novel 4-ethyl acridine-1,3,9 (2,4,10*H*)-trione. *Chem. Phys. Impact* **2024**, *8*, 100476, https://doi.org/10.1016/j.chphi.2024.100476.
35. Mellaoui, M.D.; Zaki, K.; Abbiche, K.; Imjjad, A.; Boutiddar, R.; Sbai, A.; Jmiai, A.; Issami, S.E.; Lamsabhi, A.M.; Zejli, H. In silico anticancer activity of isoxazolidine and isoxazolines derivatives: DFT study, ADMET prediction, and molecular docking. *J. Mol. Struct.* **2024**, *1308*, 138330, https://doi.org/10.1016/j.molstruc.2024.138330.
36. Isca, V.M.S.; Sitarek, P.; Merecz-Sadowska, A.; Małecka, M.; Owczarek, M.; Wieczfińska, J.; Zajdel, R.; Nowak, P.; Rijo, P.; Kowalczyk, T. Anticancer Effects of Abietane Diterpene 7α-Acetoxy-6β-hydroxyroyleanone from *Plectranthus grandidentatus* and Its Semi-Synthetic Analogs: An In Silico Computational Approach. *Molecules* **2024**, *29*, 1807, https://doi.org/10.3390/molecules29081807.
37. Ulutürk, M.; Karabacak Atay, Ç.; Tilki, T.; Dede, B. Structural properties, molecular modeling studies and antioxidant activities of novel benzoic acid-based azo molecules: A combined *in vitro* and *in silico* study. *J. Mol. Struct.* **2025**, *1344*, 142990, https://doi.org/10.1016/j.molstruc.2025.142990.
38. Çetin, Z.; Dede, B. Benzoin-based Schiff bases and their metal complexes: A multifaceted study integrating synthesis, quantum chemical calculations and solution-phase molecular simulations. *J. Mol. Liq.* **2025**, *439*, 128729, https://doi.org/10.1016/j.molliq.2025.128729.
39. Almansour, N.M.; Allemailem, K.S.; Abd El Aty, A.A.; Ismail, E.I.F.; Ibrahim, M.A.A. *In Silico* Mining of Natural Products Atlas (NPAtlas) Database for Identifying Effective Bcl-2 Inhibitors: Molecular Docking, Molecular Dynamics, and Pharmacokinetics Characteristics. *Molecules* **2023**, *28*, 783, https://doi.org/10.3390/molecules28020783.
40. Shimu, S.S. Computational screening and molecular docking of compounds from Traditional Chinese Medicine (TCM) by targeting DNA topoisomerase I to design potential anticancer drugs. *PLoS One* **2024**, *19*, e0310364, https://doi.org/10.1371/journal.pone.0310364.
41. Rathod, S.; Shinde, K.; Porlekar, J.; Choudhari, P.; Dhavale, R.; Mahuli, D.; Tamboli, Y.; Bhatia, M.; Haval, K.P.; Al-Sehemi, A.G.; Pannipara, M. Computational Exploration of Anti-cancer Potential of Flavonoids against Cyclin-Dependent Kinase 8: An *In Silico* Molecular Docking and Dynamic Approach. *ACS Omega* **2023**, *8*, 391-409, https://doi.org/10.1021/acsomega.2c04837.
42. Khamouli, S.; Tabish Rehman, M.; Zegheb, N.; Hussain, A.; Khan, M.A. Comprehensive in silico discovery of c-Src tyrosine kinase inhibitors in cancer treatment: A unified approach combining pharmacophore modeling, 3D QSAR, DFT, and molecular dynamics simulation. *J. King Saud Univ. Sci.* **2023**, *36*, 103076, https://doi.org/10.1016/j.jksus.2023.103076.

Publisher's Note & Disclaimer